

# Universal low-temperature behavior of the $\text{CePd}_{1-x}\text{Rh}_x$ ferromagnet

V.R. SHAGINYAN<sup>1 (a)</sup>, K.G. POPOV<sup>2</sup> and V. A. STEPHANOVICH<sup>3 (b)</sup>

<sup>1</sup> *Petersburg Nuclear Physics Institute, Gatchina, 188300, Russia*

<sup>2</sup> *Komi Science Center, Ural Division, RAS, Syktyvkar, 167982, Russia*

<sup>3</sup> *Opole University, Institute of Mathematics and Informatics, Opole, 45-052, Poland*

PACS 71.27.+a – Strongly correlated electron systems; heavy fermions

PACS 74.25.Jb – Electronic structure

**Abstract.** - The heavy-fermion metal  $\text{CePd}_{1-x}\text{Rh}_x$  evolves from ferromagnetism at  $x = 0$  to a non-magnetic state at some critical concentration  $x_c$ . Utilizing the quasiparticle picture and the concept of fermion condensation quantum phase transition (FCQPT), we address the question about non-Fermi liquid (NFL) behavior of ferromagnet  $\text{CePd}_{1-x}\text{Rh}_x$  and show that it coincides with that of both antiferromagnet  $\text{YbRh}_2(\text{Si}_{0.95}\text{Ge}_{0.05})_2$  and paramagnet  $\text{CeRu}_2\text{Si}_2$  and  $\text{CeNi}_2\text{Ge}_2$ . We conclude that the NFL behavior being independent of the peculiarities of specific alloy, is universal, while numerous quantum critical points assumed to be responsible for the NFL behavior of different HF metals can be well reduced to the only quantum critical point related to FCQPT.

The nature of quantum criticality determining the non-Fermi liquid (NFL) behavior observed in heavy-fermion (HF) metals is everyday topic of the physics of correlated electrons. A quantum critical point (QCP) can arise by suppressing the transition temperature  $T_c$  of a ferromagnetic (FM) (or antiferromagnetic (AFM)) phase to zero by tuning some control parameter  $\zeta$  other than temperature, such as pressure  $P$ , magnetic field  $B$ , or doping  $x$  as it takes place in the case of the HF ferromagnet  $\text{CePd}_{1-x}\text{Rh}_x$  [1,2] or the HF metal  $\text{CeIn}_{3-x}\text{Sn}_x$  [3]. The NFL behavior around QCPs manifests itself in various anomalies. One of them is power in  $T$  variations of the specific heat  $C(T)$ , thermal expansion  $\alpha(T)$ , magnetic susceptibility  $\chi(T)$  etc.

It is widely believed that the NFL behavior is determined by quantum phase transitions which occur at the corresponding QCP's. According to this concept, NFL behavior in this case is due to the presence of thermal and quantum fluctuations suppressing quasiparticles [4–6] so that the quantum criticality in these systems can be described by conventional theory related to a spin-density-wave instability [7] or scenarios where the heavy electrons localize at magnetic QCP's, for example, due to a destruc-

tion of the Kondo resonance [8]. Unfortunately, up to now it was not possible to describe all available experimental facts related to the NFL behavior within a single theory based on the above scenarios.

Measurements performed on the three dimensional FM  $\text{CePd}_{1-x}\text{Rh}_x$  show that around some concentration  $x = x_c \simeq 0.87 - 0.9$  the suppression of the FM phase occurs, so that this alloy is tuned from ferromagnetism at  $x = 0$  to a non-magnetic state at QCP with the critical concentration  $x_c$  [1, 2]. At  $x = x_c$ , measurements on  $\text{CePd}_{1-x}\text{Rh}_x$  show that the electronic contribution to the specific heat  $C(T)$  and the thermal expansion coefficient  $\alpha(T)$  behave as  $C(T) \propto \alpha(T) \propto \sqrt{T}$  [1, 9]. At the concentrations  $x < x_c$ ,  $C(T)/T$  shows a peak at some temperature  $T_{\max}$ , while under the application of magnetic field  $T_{\max}$  shifts to higher values [2]. Above discussed scenarios for NFL behavior [6–8] imply that its details would in particular depend on system's magnetic ground state. Namely, within these scenarios, one can assume that the NFL peculiarities of  $\text{CePd}_{1-x}\text{Rh}_x$  are to be different from those of either  $\text{CeNi}_2\text{Ge}_2$  and  $\text{CeRu}_2\text{Si}_2$  exhibiting a paramagnetic ground state [10, 11] or from those of AFM cubic HF metal  $\text{CeIn}_{3-x}\text{Sn}_x$  [3] and HF metal  $\text{YbRh}_2(\text{Si}_{0.95}\text{Ge}_{0.05})_2$  exhibiting (in measurements of  $C(T)/T$ ) a weak AFM ordering at  $T < 20$  mK [12]. On the other hand, the measurements of  $\chi(T)$  have shown that the quantum critical fluctuations in this metal have a

<sup>(a)</sup> Email: vrshag@thd.pnpi.spb.ru

<sup>(b)</sup> Email: stef@math.uni.opole.pl and Homepage: <http://cs.uni.opole.pl/~stef>

strong FM component and thus are unique among all other quantum critical HF systems [13]. Obviously the critical fluctuations taking place at QCPs in the different HF metals are different so that it may seem that we cannot have a universal behavior in these metals. Also, the above traditional scenarios have no grounds to consider these QCPs as different manifestations of some single QCP. Moreover, the behavior of  $C(T)/T$  in  $\text{YbRh}_2(\text{Si}_{0.95}\text{Ge}_{0.05})_2$  is formed by AFM fluctuations while that of  $\chi(T)$  is determined by FM ones. The distinctive features of FM, AFM and paramagnetic systems suggest the intrinsic differences in their QCPs resulting in the diversity of their thermodynamic properties. Existing theories corroborate this point of view, they predict that magnetic and thermal properties of  $\text{CePd}_{1-x}\text{Rh}_x$  [1,2,4–6,14] should differ from those of  $\text{YbRh}_2(\text{Si}_{0.95}\text{Ge}_{0.05})_2$  since the latter substance is supposed to combine FM and AFM orders.

Below we shall see that NFL properties of the function  $C(T)/T$  in  $\text{CePd}_{1-x}\text{Rh}_x$  coincide with those of  $\chi(T)$  in  $\text{CeRu}_2\text{Si}_2$  and  $\text{YbRh}_2(\text{Si}_{0.95}\text{Ge}_{0.05})_2$  as well as with those of  $C(T)/T$  in  $\text{YbRh}_2(\text{Si}_{0.95}\text{Ge}_{0.05})_2$ . Also, the NFL behavior of  $\alpha(T)$  in  $\text{CePd}_{1-x}\text{Rh}_x$  coincides with that of  $\alpha(T)$  in HF metals  $\text{CeNi}_2\text{Ge}_2$  and  $\text{CeIn}_{3-x}\text{Sn}_x$ . The observed power laws and universal behavior of  $C(T)$  and  $\alpha(T)$  in  $\text{CePd}_{1-x}\text{Rh}_x$  can be hardly accounted for within the above scenarios when quasiparticles are suppressed, for there is no reason to expect that  $C(T)$ ,  $\chi(T)$ ,  $\alpha(T)$  and other thermodynamic quantities are affected by the fluctuations or localization in a correlated fashion.

It might be possible to explain this universal behavior by Landau Fermi liquid (LFL) theory based on the existence of quasiparticles since  $C(T)/T \propto \alpha(T) \propto \chi(T) \propto M^*$  where  $M^*$  is the effective mass. Unfortunately, the effective mass of conventional Landau quasiparticles is temperature, magnetic field, pressure etc. independent [15] and this fact contradicts to the measurements on HF metals. On the other hand, when the electronic system of HF metals undergoes the fermion condensation quantum phase transition (FCQPT), the fluctuations are strongly suppressed and cannot destroy the quasiparticles which survive down to the lowest temperatures [16–19]. In contrast to the conventional  $M^*$ , the effective mass of these quasiparticles strongly depends on  $T$ ,  $x$ ,  $B$  etc. so that we have every reason to suggest that they are indeed responsible for the universal behavior observed in HF metals. We note that the direct observations of quasiparticles in  $\text{CeCoIn}_5$  have been reported recently [20].

In this Letter we show that the NFL properties of HF metals coincide regardless of their magnetic ground state properties. Namely, the NFL features observed in FM  $\text{CePd}_{1-x}\text{Rh}_x$ , in cubic AFM  $\text{CeIn}_{3-x}\text{Sn}_x$ , in paramagnets  $\text{CeNi}_2\text{Ge}_2$  and  $\text{CeRu}_2\text{Si}_2$  and in  $\text{YbRh}_2(\text{Si}_{0.95}\text{Ge}_{0.05})_2$  displaying both AFM and FM fluctuations, coincide. Our main conclusion is that observed universal behavior is independent of the peculiarities of the given alloy such as its lattice structure, magnetic ground state, dimensionality etc. so that numerous previously introduced QCPs can

be substituted by the only QCP related to FCQPT.

The schematic phase diagram of the HF metals under consideration is reported in fig. 1. We show two LFL regions (left one being paramagnet (PM) or having long-range magnetic order and right one corresponds to reentrant LFL phase induced by a magnetic field), separated by NFL one. The control parameter  $\zeta$  (see also above) can be pressure  $P$ , magnetic field  $B$ , or doping  $x$ . The variation of  $\zeta$  drives the system from LFL region to NFL one and then again to LFL. The caption "Magnetic field induced LFL" means that only magnetic field can generate the reentrant LFL phase. If  $\zeta$  is not a magnetic field, the right LFL-NFL boundary lies on the abscissa axis.

To study the universal low temperature features of HF metals, we use the model of homogeneous heavy-electron liquid with the effective mass  $M^*(T, B, \rho)$ , where the number density  $\rho = p_F^3/3\pi^2$ , and  $p_F$  is the Fermi momentum [15]. This permits to avoid complications associated with the crystalline anisotropy of solids [17]. To describe the effective mass  $M^*(T, B)$  as a function of temperature and applied magnetic field  $B$ , when the heavy-electron system evolves from the LFL state, we use the Landau equation relating the effective mass  $M^*(T, B)$  to the bare mass  $M$  and Landau interaction amplitude  $F(\mathbf{p}_1, \mathbf{p}_2, \rho)$  [15]

$$\frac{1}{M} = \frac{1}{M^*(T, R)} + \int \frac{\mathbf{p}_F}{p_F^2} \frac{\partial F(\mathbf{p}_F, \mathbf{p}, \rho)}{\partial \mathbf{p}_F} n(\mathbf{p}, T, R) \frac{d\mathbf{p}}{(2\pi)^3}, \quad (1)$$

where  $n(\mathbf{p}, T, R)$  is the quasiparticle distribution function

$$n(\mathbf{p}, T, R) = \frac{n(\xi + R) + n(\xi - R)}{2}, \quad (2)$$

$$n(\xi \pm R) = \left\{ 1 + \exp \left[ \frac{\xi \pm R}{T} \right] \right\}^{-1}, \quad (3)$$

$R = \mu_B B/T$ . Here  $\xi = \varepsilon(\mathbf{p}, T) - \mu$ ,  $\mu_B$  is the Bohr magneton,  $\varepsilon(\mathbf{p}, T)$  is the single-particle energy and  $\mu$  stands for a chemical potential.

We first consider the case when at  $T \rightarrow 0$  the heavy-electron liquid behaves as LFL and is located on the Fermi-liquid (FL) side of FCQPT (see Ref. [18] for details). Since  $\varepsilon(p = p_F) = \mu$  at  $B \rightarrow 0$ , we see from eq. (3) that  $n(\mathbf{p}, T, B) \rightarrow \theta(p_F - p)$ ,  $\theta(p)$  is the step function. In this case eq. (1) reads [15, 21]

$$M^*(\rho) = \frac{M}{1 - N_0 F^1(p_F, p_F, \rho)/3}. \quad (4)$$

Here  $N_0$  is the density of states of a free electron gas,  $F^1(p_F, p_F, \rho)$  is the  $p$ -wave component of Landau amplitude. LFL theory implies that the amplitude can be represented as a function of  $\rho$  only,  $F^1(p_F, p_F, \rho) = F^1(\rho)$ . We assume that at  $\rho \rightarrow \rho_{FC}$ ,  $F^1(\rho)$  achieves some value where the denominator tends to zero and find from eq. (4) that the effective mass diverges as [22, 23]

$$M^*(\rho) \simeq A + \frac{A_1}{\rho_{FC} - \rho}, \quad (5)$$

where  $A, A_1$  are constants and  $\rho_{\text{FC}}$  is QCP of FCQPT. Assuming that the control parameter  $\zeta$  is represented by  $x$  and  $x_c$  corresponds to  $\rho_{\text{FC}}$  we obtain  $(\zeta_{\text{FC}} - \zeta)/\zeta_{\text{FC}} = (x_c - x)/x_c \simeq (\rho_{\text{FC}} - \rho)/\rho_{\text{FC}}$ , while at  $\zeta > \zeta_{\text{FC}}$  the system is on the fermion condensation (FC) side of FCQPT [18].

Now we consider the temperature behavior of the effective mass  $M^*(T)$  in a zero magnetic field. Upon using eq. (4) and introducing the function  $\delta n(\mathbf{p}, T) = n(\mathbf{p}, T) - \theta(p_F - p)$ , eq. (1) takes the form

$$\frac{1}{M^*(T)} = \frac{1}{M^*(\rho)} - \int \frac{\mathbf{p}_F}{p_F^2} \frac{\partial F(\mathbf{p}_F, \mathbf{p}, \rho)}{\partial \mathbf{p}_F} \delta n(\mathbf{p}, T) \frac{d\mathbf{p}}{(2\pi)^3}. \quad (6)$$

We integrate the second term on the right hand side of eq. (6) over the angular variable  $\Omega$ , use the notation

$$F_1(p_F, p, \rho) = M p_F \int \mathbf{p}_F \frac{\partial F(\mathbf{p}_F, \mathbf{p}, \rho)}{\partial \mathbf{p}_F} \frac{d\Omega}{(2\pi)^3}, \quad (7)$$

and substitute the variable  $p$  by  $z = \xi(p)/T$ . Since in HF metals the band is flat and narrow, we use the approximation  $\xi(p) \simeq p_F(p - p_F)/M^*(T)$  and with respect to eq. (6) finally obtain

$$\frac{M}{M^*(T)} = \frac{M}{M^*(\rho)} - \beta \int_0^\infty \frac{f(1 + \beta z)}{1 + e^z} dz + \beta \int_0^{1/\beta} \frac{f(1 - \beta z)}{1 + e^z} dz, \quad (8)$$

Here  $\beta = TM^*(T)/p_F^2$  and  $f(z) = F_1(p_F, z, \rho)$ . The momentum  $p_F$  is defined from the relation  $\varepsilon(p_F) = \mu$ .

To investigate the low temperature behavior of  $M^*(T)$ , we evaluate the integral (8). Going beyond the usual approximation [24], we may obtain following final result

$$\begin{aligned} \frac{M}{M^*(T)} &= \frac{M}{M^*(\rho)} + \beta f(0) \ln \{1 + \exp(-1/\beta)\} \\ &+ \lambda_1 \beta^2 + \lambda_2 \beta^4 + \dots, \end{aligned} \quad (9)$$

where  $\lambda_1$  and  $\lambda_2$  are constants of order unity. Here the logarithmic term is the result of an effective summation of the main nonanalytic (at  $T \rightarrow 0$ ) contributions, proportional to  $\exp(-1/\beta)$ . To analyze eq. (9), we first assume that  $\beta \ll 1$ . Then, omitting terms of the order of  $\exp(-1/\beta)$ , we obtain that at  $T \ll T_F \sim p_F^2/M^*(\rho)$  the sum on the right hand side represents a  $T^2$ -correction to  $M^*(\rho)$  and the system demonstrates the LFL behavior [25]. At higher temperatures, the system enters a transition regime when the effective mass reaches its maximal value  $M_M^*$  at some temperature  $T_M$ . It can be easily checked that the terms proportional to  $\beta^2$  and  $\beta^4$  in eq. (9) are "responsible" for the maximum. The normalized effective mass  $M_N^*(T) = M^*(T)/M_M^*$  as a function of normalized temperature  $T_N = T/T_M$  is reported in the inset to fig. 1, showing several regimes. At  $T_N \ll 1$ , the LFL regime with almost constant effective mass, occurs. At  $T_N \sim 1$  it gives place to the transition region. At elevated temperatures when  $M/M^*(\rho) \ll \beta^2$ , eq. (9) reads  $M/M^*(T) \propto T^2 M^*(T)^2$ , giving [25, 26]

$$M^*(T) \propto T^{-2/3}. \quad (10)$$

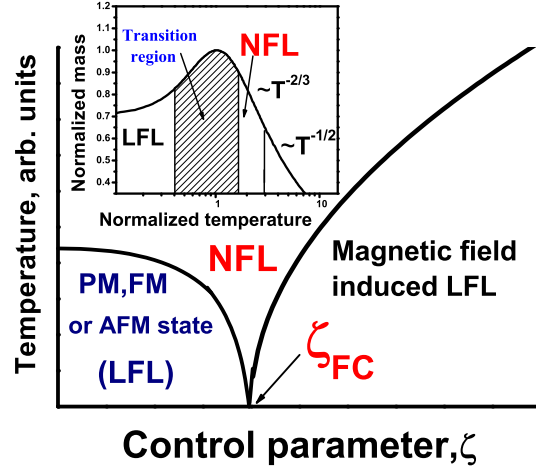


Fig. 1: Schematic phase diagram of the systems under consideration. Control parameter  $\zeta$  represents doping  $x$ , magnetic field  $B$ , pressure  $P$  etc.  $\zeta_{\text{FC}}$  denotes point at which the effective mass diverges. If  $\zeta$  is not a magnetic field, then the right boundary line NFL-LFL lies on the abscissa axis. Inset - normalized effective mass  $M_N^*(T) = M^*(T)/M_M^*$  ( $M_M^*$  is its maximal value at  $T = T_M$ ) versus the normalized temperature  $T_N = T/T_M$ . Several regions are shown. First goes the LFL regime ( $M_N^*(T) \sim \text{const}$ ) at  $T_N \ll 1$ , then transition regime (shaded area) where  $M_N^*(T)$  reaches its maximum. At elevated temperatures  $T^{-2/3}$  regime given by eq. (10) occurs followed by  $T^{-1/2}$  behavior, see eq. (11).

Numerical calculations based on eqs. (8) and (9) show that at rising temperatures the linear term  $\propto \beta$  gives the main contribution and leads to new regime when eq. (9) reads  $M/M^*(T) \propto \beta$  yielding

$$M^*(T) \propto T^{-1/2}. \quad (11)$$

Note, that "rising temperatures" are still sufficiently low for the expansion of integrals in eq. (8) in powers of  $\beta$  to be valid. In the inset to fig. 1 both  $T^{-2/3}$  and  $T^{-1/2}$  regimes are marked as NFL ones since the effective mass depends strongly on temperature, which is not the case for the transition region. If the system is located at the FCQPT critical point, it follows from eq. (5) that  $M^*(\rho_{\text{FC}}) \rightarrow \infty$  and  $T_F \rightarrow 0$  making the LFL region vanish, while the behavior of the effective mass at finite temperatures is given by eq. (11) [27]. The application of magnetic field restores the LFL behavior and at  $T = 0$  the effective mass depends on  $B$  as [26, 28]

$$M^*(B) \propto (B - B_{c0})^{-2/3}, \quad (12)$$

where  $B_{c0}$  is the critical magnetic field driving both HF metal to its magnetic field tuned QCP and corresponding Néel temperature toward  $T = 0$ . In some cases  $B_{c0} = 0$ . For example, the HF metal  $\text{CeRu}_2\text{Si}_2$  is characterized by  $B_{c0} = 0$  and shows neither evidence of the magnetic ordering or superconductivity nor the LFL behavior down to the lowest temperatures [11]. In our simple model  $B_{c0}$  is

taken as a parameter. At elevated temperatures and fixed magnetic field, the effective mass depends on temperature as in the case when the system is placed on the FL side in accordance with eqs. (10) and (11) [25, 29]. Since the magnetic field enters eq. (1) as the ratio  $R = \mu_B B/T$ , at  $T_N \lesssim 1$  the behavior of the effective mass can be described by a simple function

$$\frac{M^*(B, T)}{M^*(B)} \approx \frac{1 + c_1 \mathcal{R}^2}{1 + c_2 \mathcal{R}^{8/3}}, \quad (13)$$

which represents an approximation to solutions of eq. (1) that agrees with eqs. (10) and (12). Here  $\mathcal{R} = T/[(B - B_{c0})\mu_B]$ ,  $c_1$  and  $c_2$  are fitting parameters. As we have seen the effective mass reaches its maximal value  $M_M^*$  at some  $\mathcal{R} = \mathcal{R}_M$  and we again define a normalized effective mass as  $M_N^*(T, B) = M^*(T, B)/M_M^*$ . Taking into account eq. (13) and introducing the variable  $y = \mathcal{R}/\mathcal{R}_M$  we obtain the function

$$M_N^*(y) \approx \frac{M^*(B)}{M_M^*} \frac{1 + c_1 y^2}{1 + c_2 y^{8/3}}, \quad (14)$$

which describes a universal behavior of the effective mass  $M_N^*(y)$  when the system transits from LFL regime to that described by eq. (11). At  $\rho < \rho_{FC}$ ,  $M^*(\rho)$  is finite, see eq. (5). In this case the eq. (14) is valid at  $T_N \lesssim 1$  if  $M^*(T, B)/M^*(\rho) \ll 1$  because the term  $1/M^*(\rho)$  on the right hand side of eq. (6) is small and can be safely omitted [27]. As a result, the behavior of  $M_N^*(y)$  has to coincide with that of the normalized effective mass  $M_N^*(T)$  displayed in the inset to fig. 1.

The effective mass  $M^*(T, B)$  can be measured in experiments on HF metals. For example,  $M^*(T, B) \propto C(T)/T \propto \alpha(T)/T$  and  $M^*(T, B) \propto \chi_{AC}(T)$  where  $\chi_{AC}(T)$  is ac magnetic susceptibility. If the corresponding measurements are carried out at fixed magnetic field  $B$  (or at fixed both the concentration  $x$  and  $B$ ) then, as it follows from eq. (13), the effective mass reaches the maximum at some temperature  $T_M$ . Upon normalizing both the effective mass by its peak value at each field  $B$  and the temperature by  $T_M$ , we observe that all the curves merge into single one, given by eq. (14) thus demonstrating a scaling behavior.

As it is seen from fig. 2, the behavior of the normalized ac susceptibility  $\chi_N^*(y) = \chi_{AC}(T/T_M, B)/\chi_{AC}(1, B) = M_N^*(T_N)$  obtained in measurements on the HF paramagnet  $\text{CeRu}_2\text{Si}_2$  [11] agrees with both the approximation given by eq. (14) and the normalized specific heat  $(C(T_N)/T_N)/C(1) = M_N^*(T_N)$  obtained in measurements on the HF FM  $\text{CePd}_{1-x}\text{Rh}_x$  [2]. It is also seen from fig. 2, that at temperatures  $T_N \leq 3$ , the curve given by eq. (14) agrees perfectly with the measurements on  $\text{CeRu}_2\text{Si}_2$  whose electronic system is placed at FCQPT [29], that is in fig. 1 at  $\zeta_{FC}$ . As to the normalized specific heat (shown by downright triangles in fig. 2) measured on  $\text{CePd}_{1-x}\text{Rh}_x$  with  $x = 0.8$  [2], the scaling holds up to relatively high temperatures. This is because its elec-

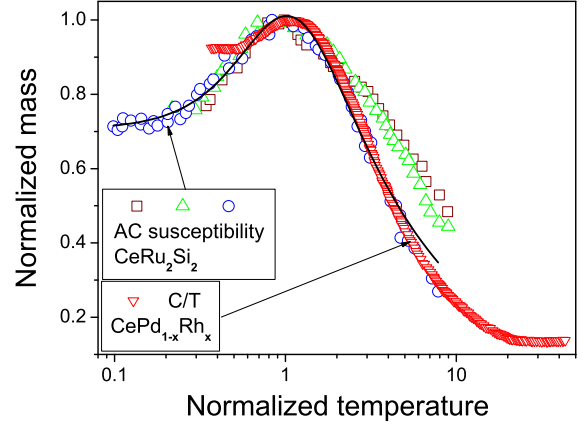


Fig. 2: Normalized magnetic susceptibility  $\chi_N(T_N, B) = \chi_{AC}(T/T_M, B)/\chi_{AC}(1, B) = M_N^*(T_N)$  for  $\text{CeRu}_2\text{Si}_2$  in magnetic fields 0.20 mT (squares), 0.39 mT (upright triangles) and 0.94 mT (circles) against normalized temperature  $T_N = T/T_M$  [11]. The susceptibility reaches its maximum  $\chi_{AC}(T_M, B)$  at  $T = T_M$ . The normalized specific heat  $(C(T_N)/T_N)/C(1)$  of the HF ferromagnet  $\text{CePd}_{1-x}\text{Rh}_x$  with  $x = 0.8$  versus  $T_N$  is shown by downright triangles [2]. Here  $T_M$  is the temperature at the peak of  $C(T)/T$ . The solid curve traces the universal behavior of the normalized effective mass determined by eq. (14), it is also shown in figs. 3, 4, 5 and 6. Parameters  $c_1$  and  $c_2$  are adjusted for  $\chi_N(T_N, B)$  at  $B = 0.94$  mT.

tronic system is located on the FL side and the deflection  $(x_c - x)/x_c \simeq (\rho - \rho_{FC})/\rho_{FC}$  at  $x = 0.8$  from the critical concentration  $x_c \simeq 0.9$  is relatively big, elongating the  $T^{-2/3}$  region [27]. On the other hand, at diminishing temperatures the scaling is ceased at relatively high temperatures as soon as the LFL behavior related to the deflection from  $x_c$  sets in.

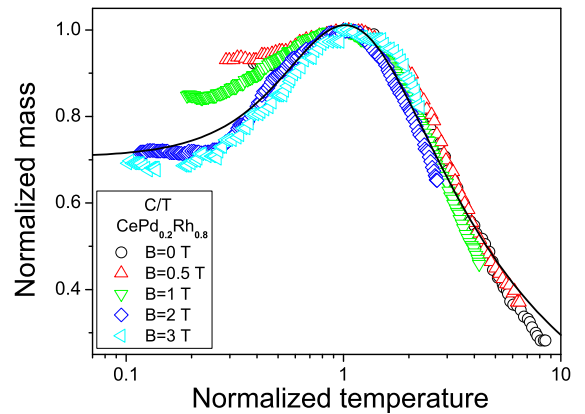


Fig. 3: The normalized effective mass  $M_N^*(T_N, B)$  extracted from the measurements of the specific heat on  $\text{CePd}_{1-x}\text{Rh}_x$  with  $x = 0.8$  [2]. At  $B \geq 1$  T,  $M_N^*(T_N)$  coincides with that of  $\text{CeRu}_2\text{Si}_2$  (solid curve, see the caption to fig. 2).

Now we consider the behavior of  $M_N^*(T)$ , extracted from measurements of the specific heat on  $\text{CePd}_{1-x}\text{Rh}_x$  under



the application of magnetic field [2] and shown in fig. 3. It is seen from fig. 3 that at  $B \geq 1\text{ T}$  the value  $M_N^*$  describes the normalized specific heat almost perfectly, coincides with that of  $\text{CeRu}_2\text{Si}_2$  and is in accord with the universal behavior of the normalized effective mass given by eq. (14). Thus, we conclude that the thermodynamic properties of  $\text{CePd}_{1-x}\text{Rh}_x$  with  $x = 0.8$  are determined by quasiparticles rather than by the critical magnetic fluctuations. On the other hand, one could expect the growth of the critical fluctuations contribution as  $x \rightarrow x_c$  so that the behavior of the normalized effective mass would deviate from that given by eq. (14).

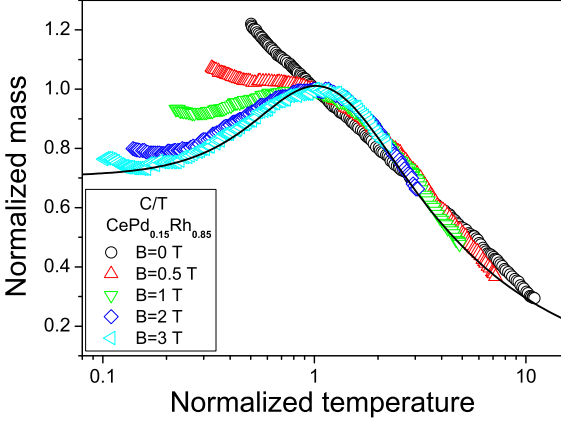


Fig. 4: Same as in Fig. 3 but  $x = 0.85$  [2]. At  $B \geq 1\text{ T}$ ,  $M_N^*(T_N)$  demonstrates the universal behavior (solid curve, see the caption to fig. 2).

In fig. 4, the effective mass  $M_N^*(T_N)$  at fixed  $B$ 's is shown. Since the curve shown by circles and extracted from measurements at  $B = 0$  does not exhibit any maximum down to  $0.08\text{ K}$  [2], we conclude that in this case  $x$  is very close to  $x_c$  and function  $M_N^*(T_N)$  is approximately described by eq. (11), while the maximum is shifted to very low temperatures or even absent. As seen from fig. 4, the application of magnetic field restores the universal behavior given by eq. (14). Again, this permits us to conclude that thermodynamic properties of  $\text{CePd}_{1-x}\text{Rh}_x$  with  $x = 0.85$  are determined by quasiparticles rather than by the critical magnetic fluctuations.

The thermal expansion coefficient  $\alpha(T)$  is given by [24]  $\alpha(T) \simeq M^*T/(p_F^2 K(\rho))$ . The compressibility  $K(\rho)$  is not expected to be singular at FCQPT and is approximately constant [30]. Taking into account eq. (11), we find that  $\alpha(T) \propto \sqrt{T}$  and the specific heat  $C(T) = TM^* \propto \sqrt{T}$ . Measurements of the specific heat  $C(T)$  on  $\text{CePd}_{1-x}\text{Rh}_x$  with  $x = 0.9$  show a power-law temperature dependence. It is described by the expression  $C(T)/T = AT^{-q}$  with  $q \simeq 0.5$  and  $A = \text{const}$  [1]. Hence, we conclude that the behavior of the effective mass given by eq. (11) agrees with experimental facts. Measurements of  $\alpha(T)/T$  on both  $\text{CePd}_{1-x}\text{Rh}_x$  with  $x = 0.9$  [1] and  $\text{CeNi}_2\text{Ge}_2$  [10] are shown in fig. 5. It is seen that the approxima-

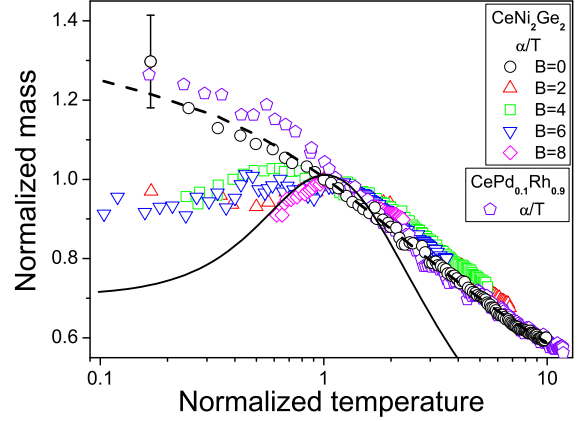


Fig. 5: The normalized thermal expansion coefficient  $(\alpha(T_N)/T_N)/\alpha(1) = M_N^*(T_N)$  for  $\text{CeNi}_2\text{Ge}_2$  [10] and for  $\text{CePd}_{1-x}\text{Rh}_x$  with  $x = 0.90$  [2] versus  $T_N = T/T_M$ . Data obtained in measurements on  $\text{CePd}_{1-x}\text{Rh}_x$  at  $B = 0$  are multiplied by some factor to adjust them in one point to the data for  $\text{CeNi}_2\text{Ge}_2$ . Dashed line is a fit for the data shown by the circles and pentagons at  $B = 0$  and represented by the function  $\alpha(T) = c_3\sqrt{T}$  with  $c_3$  being a fitting parameter. The solid curve traces the universal behavior of the normalized effective mass determined by eq. (14), see the caption to fig. 2.

tion  $\alpha(T) = c_3\sqrt{T}$  is in good agreement with the results of measurements of  $\alpha(T)$  in  $\text{CePd}_{1-x}\text{Rh}_x$  and  $\text{CeNi}_2\text{Ge}_2$  over two decades in  $T_N$ . We note that measurements on  $\text{CeIn}_{3-x}\text{Sn}_x$  with  $x = 0.65$  [3] demonstrate the same behavior  $\alpha(T) \propto \sqrt{T}$  (not shown in fig. 5). As a result, we suggest that  $\text{CeIn}_{3-x}\text{Sn}_x$  with  $x = 0.65$ ,  $\text{CePd}_{1-x}\text{Rh}_x$  with  $x \simeq 0.9$ , and  $\text{CeNi}_2\text{Ge}_2$  are located at FCQPT (in fig. 1 at  $\zeta_{\text{FC}}$ ) and recollect that  $\text{CePd}_{1-x}\text{Rh}_x$  is a three dimensional FM [1, 2],  $\text{CeNi}_2\text{Ge}_2$  exhibits a paramagnetic ground state [10] and  $\text{CeIn}_{3-x}\text{Sn}_x$  is AFM cubic metal [3].

$M_N^*(T_N)$  extracted from measurements on the HF metals  $\text{YbRh}_2(\text{Si}_{0.95}\text{Ge}_{0.05})_2$ ,  $\text{CeRu}_2\text{Si}_2$ ,  $\text{CePd}_{1-x}\text{Rh}_x$  and  $\text{CeNi}_2\text{Ge}_2$  is reported in fig. 6. It is seen that the universal behavior of the effective mass given by eq. (14) is in accord with experimental facts.  $\text{YbRh}_2(\text{Si}_{0.95}\text{Ge}_{0.05})_2$  is located on the FC side where the system demonstrates the NFL behavior down to lowest temperatures [27]. In that case,  $\zeta$  (see fig. 1) is represented by  $B$  and  $\zeta_{\text{FC}} = B_{c0}$ . In the LFL regime induced by the magnetic field, the effective mass  $M^*(B) \propto (B - B_{c0})^{-1/2}$  and does not follow eq. (12) [27, 29]. As a result, the range of the scaling behavior in temperature shrinks to the transition and  $T^{-2/3}$  regions, see inset to fig. 1. It is seen from fig. 6 that  $M_N^*(T_N)$  shown by downright triangles and collected on the AFM phase of  $\text{YbRh}_2(\text{Si}_{0.95}\text{Ge}_{0.05})_2$  [12] coincides with that collected on the FM phase (shown by upright triangles) of  $\text{YbRh}_2(\text{Si}_{0.95}\text{Ge}_{0.05})_2$  [13]. We note that in the case of LFL theory the corresponding normalized effective mass  $M_{NL}^* \simeq 1$  is independent of both  $T$  and  $B$ .

The peak temperatures  $T_{\text{max}}$ , where the maxima of  $C(T)/T$ ,  $\chi_{AC}(T)$  and  $\alpha(T)/T$  occur, shift to higher val-

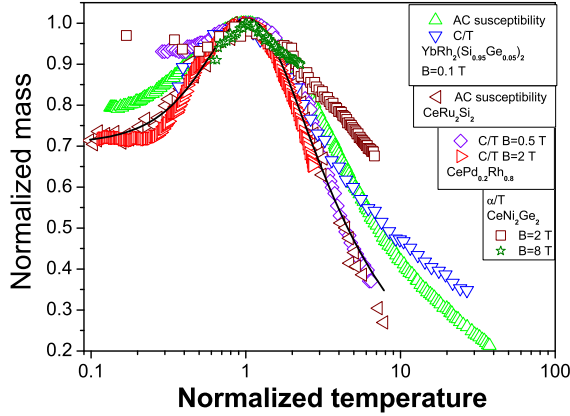


Fig. 6: The universal behavior of  $M_N^*(T_N)$ , extracted from  $\chi_{AC}(T, B)/\chi_{AC}(T_M, B)$  for both  $\text{YbRh}_2(\text{Si}_{0.95}\text{Ge}_{0.05})_2$  and  $\text{CeRu}_2\text{Si}_2$  [11, 13],  $(C(T)/T)/(C(T_M)/T_M)$  for both  $\text{YbRh}_2(\text{Si}_{0.95}\text{Ge}_{0.05})_2$  and  $\text{CePd}_{1-x}\text{Rh}_x$  with  $x = 0.80$  [2, 12], and  $(\alpha(T)/T)/(\alpha(T_M)/T_M)$  for  $\text{CeNi}_2\text{Ge}_2$  [10]. All the measurements are performed under the application of magnetic field as shown in the insets. The solid curve gives the universal behavior of  $M_N^*$  determined by eq.(14), see the caption to fig.2.

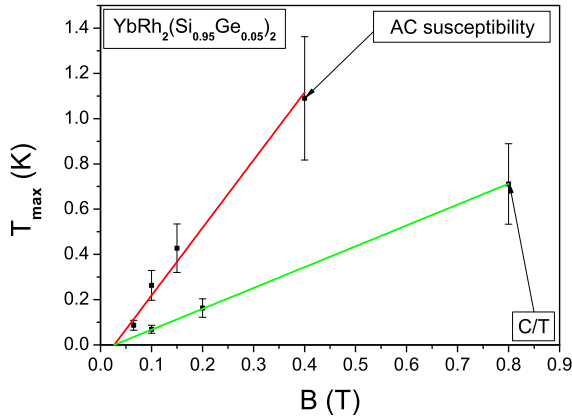


Fig. 7: The peak temperatures  $T_{\max}(B)$ , extracted from measurements of  $C/T$  and  $\chi_{AC}$  on  $\text{YbRh}_2(\text{Si}_{0.95}\text{Ge}_{0.05})_2$  [12, 13] and approximated by straight lines. The lines intersect at  $B \simeq 0.03$  T.

ues with increase of the applied magnetic field. It follows from eq. (14) that  $T_M \propto (B - B_{c0})\mu_B$ . In fig. 7,  $T_{\max}(B)$  are shown for  $C/T$  and  $\chi_{AC}$ , measured on  $\text{YbRh}_2(\text{Si}_{0.95}\text{Ge}_{0.05})_2$ . It is seen that both functions can be represented by straight lines intersecting at  $B \simeq 0.03$  T. This observation [12, 13] as well as the measurements on  $\text{CePd}_{1-x}\text{Rh}_x$ ,  $\text{CeNi}_2\text{Ge}_2$  and  $\text{CeRu}_2\text{Si}_2$  demonstrate the same behavior [2, 10, 11].

In summary, we have shown, that bringing the different experimental data (like  $C(T)/T$ ,  $\chi_{ac}(T)$ ,  $\alpha(T)/T$  etc) collected on different HF metals ( $\text{YbRh}_2(\text{Si}_{0.95}\text{Ge}_{0.05})_2$ ,  $\text{CeRu}_2\text{Si}_2$ ,  $\text{CePd}_{1-x}\text{Rh}_x$ ,  $\text{CeIn}_{3-x}\text{Sn}_x$  and  $\text{CeNi}_2\text{Ge}_2$ ) to the above normalized form immediately reveals their universal scaling behavior. This is because all above experi-

mental quantities are indeed proportional to the normalized effective mass. Since the effective mass determines the thermodynamic properties, we conclude that above alloys demonstrate the universal NFL thermodynamic behavior, independent of the details of the HF metals such as their lattice structure, magnetic ground state, dimensionality etc. This conclusion implies also that numerous QCPs assumed earlier to be responsible for the NFL behavior of different HF metals can be well reduced to a single QCP related to FCQPT.

This work was supported in part by RFBR, project No. 05-02-16085.

## REFERENCES

- [1] SERENI J. G. *et al.*, *Phys. Rev. B*, **75** (2007) 24432.
- [2] PIKUL A. P. *et al.*, *J. Phys. Condens. Matter*, **18** (2006) L535.
- [3] KÜCHLER R. *et al.*, *Phys. Rev. Lett.*, **96** (2006) 256403.
- [4] STEWART G. R., *Rev. Mod. Phys.*, **73** (2001) 797.
- [5] VOJTA M., *Rep. Prog. Phys.*, **66** (2003) 2069.
- [6] LÖHNEISEN H.V. *et al.*, unpublished (cond-mat/0606317).
- [7] MILLIS A. J., *Phys. Rev. B*, **48** (1993) 7183.
- [8] SI Q. *et al.*, *Nature*, **413** (2001) 804.
- [9] SHAGINYAN V. R., POPOV K. G., ARTAMONOV S.A., *JETP Lett.*, **85** (2007) 398.
- [10] KÜCHLER R. *et al.*, *Phys. Rev. Lett.*, **91** (2003) 066405.
- [11] TAKAHASHI D. *et al.*, *Phys. Rev. B*, **67** (2003) 180407(R).
- [12] CUSTERS J. *et al.*, *Nature*, **424** (2003) 524.
- [13] GEGENWART P. *et al.*, *Phys. Rev. Lett.*, **94** (2005) 076402.
- [14] KIRKPATRICK T. R. and BELITZ D., *Phys. Rev. B*, **67** (2003) 044419.
- [15] LIFSHITZ E. M. and PITAEVSKII L. P., *Statistical Physics, Part 2* (Butterworth-Heinemann, Oxford) 1999.
- [16] SHAGINYAN V. R., *JETP Lett.*, **79** (2004) 286.
- [17] SHAGINYAN V. R. *et al.*, *Europhys. Lett.*, **76** (2006) 898.
- [18] AMUSIA M. YA. and SHAGINYAN V. R., *Phys. Rev. B*, **63** (2001) 224507.
- [19] AMUSIA M. YA. and SHAGINYAN V. R., *JETP Lett.*, **73** (2001) 232.
- [20] PAGLIONE J. *et al.*, *Phys. Rev. Lett.*, **97** (2006) 106606.
- [21] PFITZNER M. and WÖLFLE P., *Phys. Rev. B*, **33** (1986) 2003.
- [22] SHAGINYAN V. R., *JETP Lett.*, **77** (2003) 99.
- [23] YAKOVENKO V.M. and KHODEL V.A., *JETP Lett.*, **78** (2003) 398.
- [24] LIFSHITZ E. M. and PITAEVSKII L. P., *Statistical Physics, Part 1* (Butterworth-Heinemann, Oxford) 2000.
- [25] SHAGINYAN V. R., *JETP Lett.*, **80** (2004) 263.
- [26] CLARK J. W., KHODEL V. A. and ZVEREV M. V., *Phys. Rev. B*, **71** (2005) 012401.
- [27] SHAGINYAN V. R., AMUSIA M. YA. and MSEZANE A. Z., *Phys. Lett. A*, **338** (2005) 393.
- [28] SHAGINYAN V. R., *JETP Lett.*, **77** (2003) 178.
- [29] SHAGINYAN V. R., *JETP Lett.*, **79** (2004) 286.
- [30] NOZIÈRES P., *J. Phys. I (France)*, **2** (1992) 443.